

Article

Comparison of Substrate Preheating on Mechanical and Microstructural Properties of Hybrid Specimens Fabricated by Laser Metal Deposition 316 L with Different Wrought Steel Substrate

Yuhui Zhao ^{1,2,3,*} , Zhiguo Wang ^{1,2} , Jibin Zhao ^{1,2}, Zhenfeng He ^{1,2} and Hongwei Zhang ⁴

¹ Shenyang Institute of Automation, Chinese Academy of Sciences, Shenyang 110016, China;

wangzhiguo@sia.cn (Z.W.); jbzhaos@sia.cn (J.Z.); hezhenfeng@sia.cn (Z.H.)

² Institutes for Robotics and Intelligent Manufacturing, Chinese Academy of Sciences, Shenyang 110169, China

³ University of Chinese Academy of Sciences, Beijing 100049, China

⁴ Taizhou Xinma Technology Industry Development Co., Ltd., Taizhou 225327, China;

hongweizhang@imr.ac.cn

* Correspondence: yhzhaos@sia.cn

Received: 28 August 2020; Accepted: 28 September 2020; Published: 1 October 2020



Abstract: The combination of additive manufacturing and conventional metal forming processes provides the possibility for improvements of forming efficiency and flexibility. Substrate preheating is an implementable technique to improve the interface adhesion properties of the hybrid forming method. The present experiment investigates the adhesion of additive manufactured 316 L steel on P20 and 1045 steel substrates under two substrate temperatures, and the geometrical characterization, interfacial microstructure and mechanical property of the hybrid specimens were compared. As a result, it was found that the ratio of deposition height to the width was reduced and the width was increased under substrate preheating. Tensile results show that the ultimate strength of 1045 and 316 L hybrid specimens was obviously increased, while the properties of hybrid specimens P20 and 316 L were similar, under different substrate temperature conditions. For the hybrid specimens with the metallurgically bonding characteristic, the tensile properties can reach the level of 316 L deposited specimens fabricated by laser metal deposition (LMD). Furthermore, substrate preheating had little effect on the microstructure of the laser metal deposition zone, and significant influence on the microstructure of the heat affected zone, which was reflected in the difference of the hardness distribution.

Keywords: substrate preheating; hybrid forming; geometrical characteristics; microstructure; tensile properties

1. Introduction

In order to improve the building efficiency of current forming technology, integrating additive manufacturing with conventional manufacturing (metal forming) processes is an economical way to fabricate large-scaled structures with local precision parts [1]. Some functional structures can be manufactured by building multilayer sections with laser metal deposition (LMD) on existing substrates using precision casting or wrought. This includes using a mold with conformal cooling channels [2,3], component repairing [4], and surface strengthening [5,6]. This hybrid manufacturing process has been thoroughly discussed for titanium alloy [7] and steel [8].

On the one hand, when steel is used for mold and die (especially high carbon steel), it is difficult to deposit many layers on conventional manufacturing substrate without defects, as it is an alloy with

high levels of hardness. Simultaneously, the LMD process offers the capability of depositing diverse material, such as interlayer materials [9] and functionally gradient materials [10,11]. This characteristic can be utilized to build dense deposition layers on existing substrate without cracks. For hybrid manufacturing processes, the interfacial adhesion property is in significant need of a high-reliability of industry applications. Most of the previous studies have concentrated on depositing high-hardness material with low height on conventional manufacturing steel, which was mainly used in mold repairing or surface hardening. Chen et al. discussed residual stresses during cladding the P20 tool on wrought P20 substrate [12], Liu et al. discussed laser clad AerMet100 steel coating on 300 M steel substrate [13]. Sun et al. formed an AISI 4340 steel coating on an AISI 4140 steel substrate [14]. The former studies were mainly aimed at depositing on a small area (the maximum length of deposition area was less than 1000 mm) with a small deposition height (deposition layer number was less than 10).

On the other hand, combining conventional manufacturing with the additive manufacturing process [15–17], which is also called the hybrid forming process, seems to be a reasonable method for complex mold and die forming [18]. The hardened surface region of molds and dies require high levels of hardness, which requires a significant martensite phase in microstructure. In general, the martensitic steel has poor plasticity. In consideration of deposition height, the deposition height in the hybrid forming process is usually higher than laser cladding. The residual stress increased with the increasing of deposition area and layers. This increases the tendency for cracking to occur during the deposition process, especially depositing on high-hardness material. Depositing interlayer materials with good deformation performance seems to be a useful way for safe adhesion at the interface of different materials and forming processes. This way, the residual stress at the interface can be weakened. By successive depositing of interlayer materials and surface-hardened steel on conventional manufacturing steel substrate, the hybrid formed mold can be realized. The interface adhesion properties and mechanical properties of interlayer material and conventional manufacturing steel are necessary research areas.

Many researchers have paid attention to improving the interfacial adhesion property by optimizing material composition, substrate preheating and process parameters. Among them, substrate preheating is a universal and efficient way to realize good interface adhesion when laser cladding hard material, such as high C martensite steel [19], metallic glass [20] and hypereutectoid steel [21], which has a tendency to crack because of martensite transformation or composition difference. In these studies, the preheating in laser additive manufacturing was mostly applied in surface cladding for high-hardness and easy-cracking steel.

Therefore, in consideration of interlayer material with good ductility and toughness, whether there was an effect of substrate preheating on the mechanical properties in the laser cladding process was not clear. The 316 L stainless steel was selected as the interlayer material between higher-hardness surface material and conventional manufacturing steel, which has been used as the interlayer material for hybrid formed Hot Stamping Dies [2]. In this paper, the Wrought P20 and 1045 steels formed by forging were used as the substrate material, which has the integrated mechanical properties to serve as the base region of the hybrid mold. The influence of substrate preheating on the interfacial microstructure and mechanical behavior between laser deposition interlayer material and conventional manufacturing steel was systematically analyzed.

2. Materials and Methods

Commercial 1045 and P20 wrought steel plates, with dimensions of 50 mm × 120 mm × 30 mm ($W \times L \times T$) were used as the substrate. The composition of the P20 steel was as follows: 0.004 C, 0.015 Cr, 0.008 Mn, 0.003 Si, 0.005 Mo and bal. Fe. Wrought 1045 steel was composed of 0.005 C, 0.002 Si, 0.005 Mn and bal. Fe. Prior to the deposition process, the top surface of the substrate was machined and cleaned with acetone, which was to remove the surface oxide and ensure the same surface roughness of different samples. Simultaneously, the 316 L stainless steel powders provided by Höganäs (China) Co., Ltd. (Dalian, Liaoning, China) were used as the deposition material, the composition of which was

The specimens for microstructure and geometric characterization observation were mounted, polished, then etched in chloroazotic acid. The substrate steel was etched by a nitric acid–alcohol solution for optical microscopy observation. The microstructure of those specimens was observed by stereology microscopy (Stemi 2000, Carl Zeiss AG, Oberkochen, Germany) and optical microscopy (Axiovert 200 MAT, Carl Zeiss AG, Oberkochen, Germany). Microstructure and fracture surface were observed by means of Hitachi S-3400 N (Hitachi, Tokyo, Japan) and TESCAN MAIA3 (TESCAN China, (Shanghai, China) scanning electron microscope (SEM). Elemental analysis was done by energy dispersive spectrometry (EDS) (TESCAN China, (Shanghai, China)) during the SEM analysis. Based on the guidelines given in GB/T 228.1-2010, the sizes of tensile test specimens were determined, as shown in Figure 1b. The RT (room temperature) tensile testing was conducted on the 5582 Instron testing machine (Instron, Boston, Massachusetts, USA). The hardness was measured by Vickers hardness tester (AMH43) with an indentation load of 200 g for 15 s. The residual stress was measured by a Photo-LXRD X-ray diffraction device (P’Nalytical B.V., Almelo, the Netherlands), and the testing points are marked in Figure 1.

3. Results and Discussion

3.1. Geometric Characterization

The comparison of these calculated results is listed in Figure 2. The X-axis in Figure 2 represents laser power (P) and scanning speed (S) under different combination of process parameters. As shown in Figure 2a,b, the melt height (H1) and deposition width (W1) are significantly increased under the effect of substrate preheating. However, the deposition height (H2) of specimens with substrate preheating are slightly lower or equal to the specimens without substrate preheating. Similarly, this result was also found in laser deposition of 316 L on P20 steel. Evidently, the remolten size of the substrate increased with the help of substrate preheating, which would lead to the increase of W1 and H1. The calculated results of W1, H1 and the sum of H1 and H2 are closely related to laser power and scanning speed. The sum of H1 and H2, which indicates the height of the remolten pool section, is increased as a result of the increased powder catchment efficiency [24] and remolten zone volume. However, no clear relationship between H2 and laser powder and scanning speed was found. Similarly, the variation of W1, H1 and H1 + H2 of 316 L with P20 steel substrate shows the same variation tendency with the change of process parameters (laser power and scanning speed).

The values of H2 and W1 were assessment indexes of the deposition layer. The statistical results shown in Figure 2a indicate that W1 of deposition specimens on 1045 steel substrate ranges from 3.679 to 4.207 mm among the parameters listed in Figure 2; while the range from 3.962 to 4.744 mm exists for substrate preheating, which is greater than the laser beam diameter (3 mm) as mentioned by Liu et al. [25]. The W1 ranges of the different materials deposited under various heat input is lower than the ranges when using substrate preheating. The H2 of deposition specimens on 1045 steel ranges from 0.481 to 0.792 mm and ranges from 0.489 to 0.679 mm with substrate preheating. This means H2 ranges of the different materials deposited under various heat inputs is greater than the ranges when using substrate preheating. For specimens under the same heat input, the value of W1 was increased and H2 was decreased, and the ratio of H2/W1 is decreased under substrate preheating. The H2/W1 ratios of 316 L on 1045 specimens were 0.141 (1600 W, 6 mm/s) and 0.142 (2000 W, 6 mm/s) without preheating, decreased to 0.127 and 0.121, respectively, under substrate preheating as illustrated in Figure 3a. Similarly, the H2/W1 ratios of 316 L on P20 specimens decreased to 0.118 (1600 W, 6 mm/s) and 0.109 (2000 W, 6 mm/s) under substrate preheating, from 0.131 and 0.125, respectively, as illustrated in Figure 3b. This indicates that the contact angle (illustrated in Figure 3) was reduced under the effect of substrate preheating. The contact angle was reduced under substrate preheating, which makes the top surface of the deposition layer smoother than the surface without preheating.

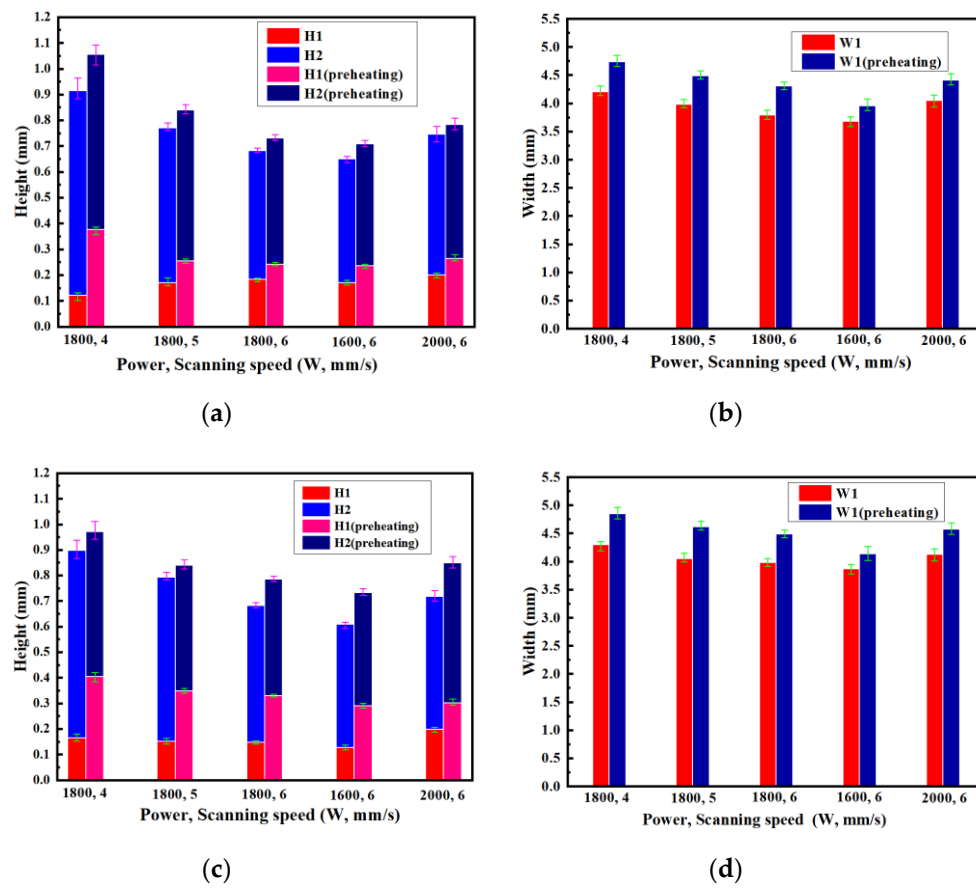


Figure 2. Effect of substrate preheating on calculated results under different process parameters: (a) height of 1045/316 L; (b) width of 1045/316 L; (c) height of P20/316 L; (d) width of P20/316 L.

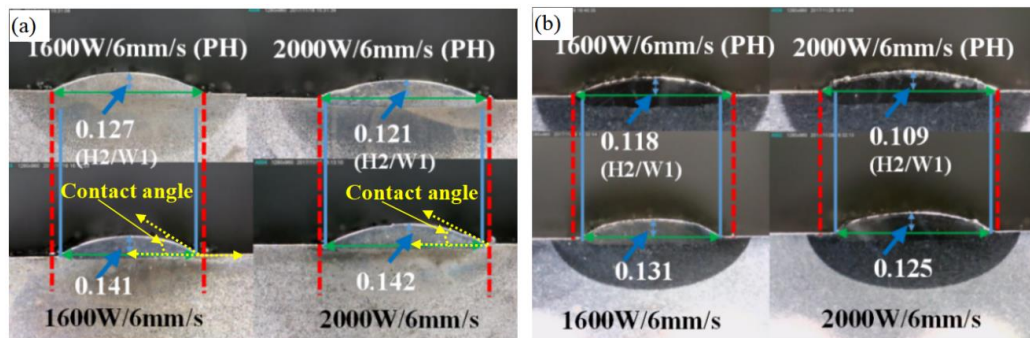


Figure 3. Morphology of laser metal deposition 316 L on 1045 steel (a) and P20 steel (b).

3.2. Macrostructure Analysis

Figure 4a,c shows micrographs of hybrid specimens made by LMD 316 L with 1045 and P20 steel, respectively, LMD 316 L with 1045 and P20 steel specimens with substrate preheating are also respectively shown in Figure 4b,d for comparison. The deposition boundaries are marked by red and yellow lines in Figure 4. The deposition boundaries of zigzag structure became the adjacent layer, scanning along the opposite direction. As shown in Figure 4b, LMD 316 L formed metallurgically sound and dense bonding with 1045 steel under substrate preheating, while defects formed near the bonding interface and terminated on the bottom melting line of the third deposition layer without substrate preheating. Unmolten powder was found in the defects zone as shown in Figure 5b, which verifies the insufficient bonding behavior. Meanwhile, internal stress caused cracking near the interface, as marked by the yellow dash line Figure 5c. The difference in interface morphology was mainly due to the

morphology of the deposition layer. Assuming the wider deposition width of the single scanning path and the smoother surface morphology of one deposition layer under the substrate preheating, the insufficient bonding behavior between adjacent layers of multiple layers was eliminated. However, both LMD 316 L with P20 steel specimens have metallurgically bonding characteristics without defects under different substrate temperatures. Defects were generated by insufficient bonding between the adjacent deposition tracks. Comparing the difference of deposition width between 1045 and P20 steel as shown in Figure 2b,d, it is evident that the deposition width on 1045 steel is slightly smaller than P20 steel under the same parameter. The boundaries of different deposition tracks are clearly distinguished in Figure 4a,c. The height of the deposition track with substrate preheating is larger than other tracks. This phenomenon is more clearly evident in LMD 316 L with P20 steel.

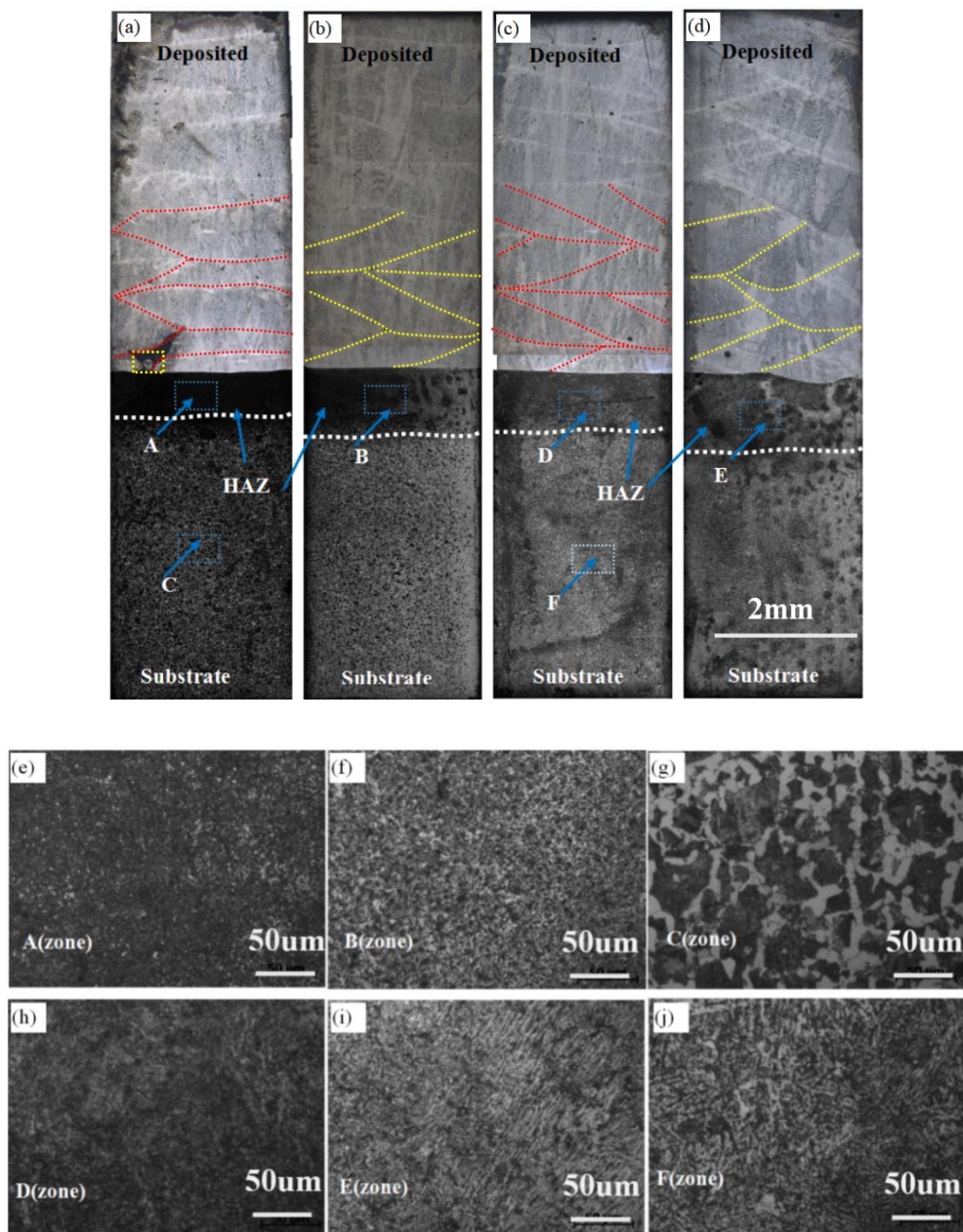


Figure 4. Optical macrograph showing the morphologies on the transverse cross section of (a) 316 L with 1045 without preheating, (b) 316 L with P20 without preheating, (c) 316 L with 1045 preheated to 200 °C, (d) 316 L with P20 preheated to 200 °C; microstructure of A zone (e), B zone (f), C zone (g), D zone (h), E zone (i), F zone (j).

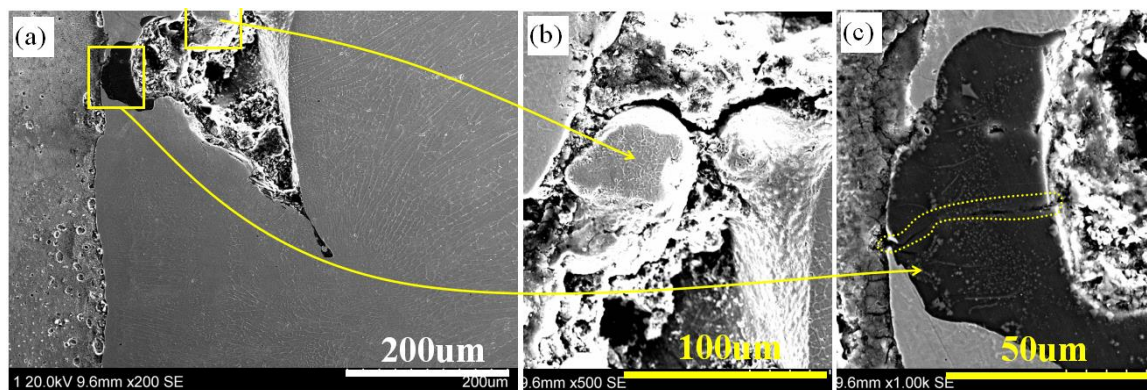


Figure 5. SEM micrographs near the defects zone: (a) defects near interface; (b) unmolten powder; (c) crack zone.

3.3. Interfacial Morphology

Figure 6 presents the microstructural characteristics of the interface between 316 L deposition layer with 1045 and P20 substrate. As shown in Figure 6, the flat structure is presented at the interface under the effect of high temperature gradient and low solidification velocity. Fine cellular and columnar dendritic have grown perpendicular to the interface, which was caused by temperature gradient perpendicular to the bottom of the molten pool. The microstructure of laser metal deposition 316 L is mainly composed of δ , γ phases, as reported in the literature [26,27]. The matrix phase (dark region in the dendritic region) is the γ austenite phase, and the interdendritic phase is δ -ferrite or γ -austenite in reticular distribution morphology. However, it is difficult to distinguish the δ -ferrite from the SEM images. In comparison to the deposition microstructure, it is apparent that the microstructure morphology of the deposition layer is similar. The average dendrite arm space of the microstructure with different substrate temperatures is below 10 μm , while the dendrite arm space only minorly increased with the increasing substrate temperature. The impacts of substrate preheating on the microstructure of the deposition layer is mild.

Nevertheless, the microstructure of the HAZ (heat affected zone) in the substrate is different between the microstructure of different substrate temperatures. The difference is also found in specimens of both of 316 L with 1045 and P20 substrate. The unaffected microstructure of 1045 steel consisting of ferrite and pearlite is shown in Figure 7a; the ferrite is the dark phase etched by a nitric acid–alcohol solution; and the pearlite phase consists of alternating layers of ferrite (dark region) and cementite (white phase in long strips). This is consistent with the optical result as shown in Figure 4g, the white zone is the ferrite, and the dark zone is pearlite. During laser deposition, the ferrite and pearlite austenitized, cooled rapidly, and then formed a nonequilibrium microstructure during the cooling process. Rashid et al. [28] reported the HAZ microstructure of mild steel during laser deposition consisted of martensitic lath plus ferrite and bainite plus ferrite. The resulting HAZ microstructure is affected by peak temperature and cooling rate [29], which is closely related to the processing parameters and substrate properties. The resultant microstructure within the scope of this research mainly consists of pearlite in different morphologies, and the microstructure is refined. The composition of the ferrite phase in the HAZ is obviously decreased as shown in Figure 4e,f. The HAZ microstructure of 1045 steel under substrate preheating is coarsened with preheating.

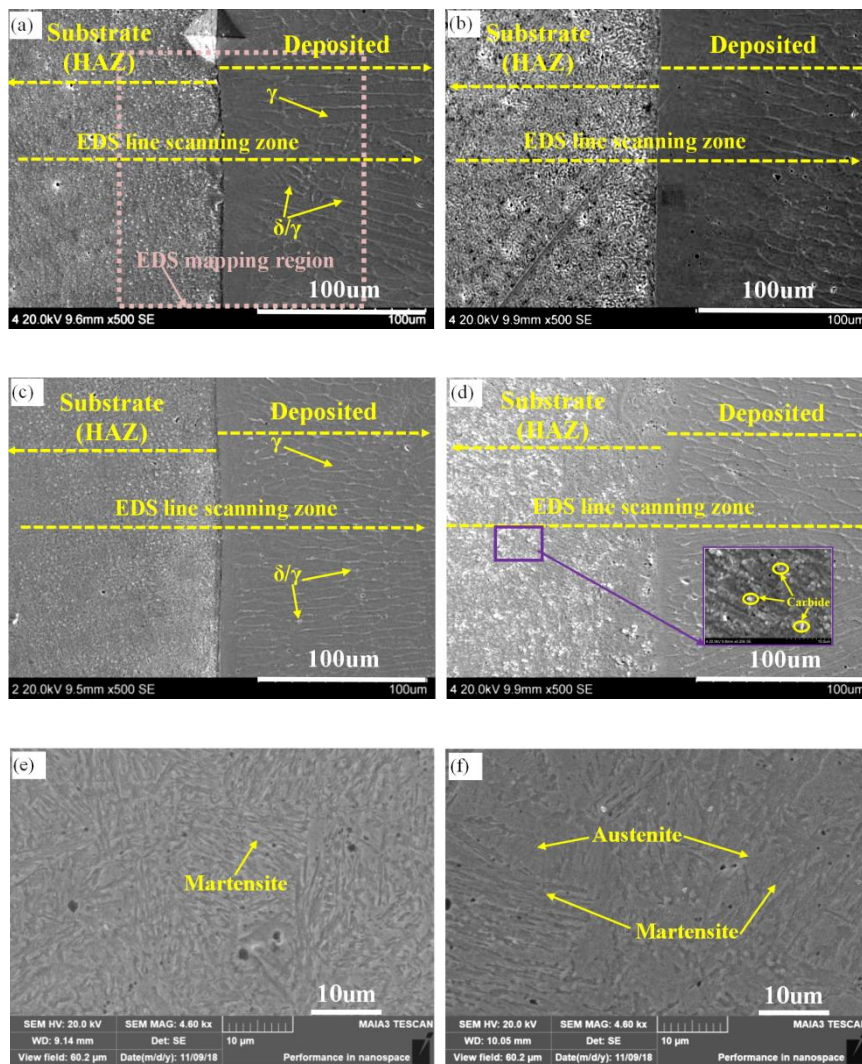


Figure 6. Microstructure of the cross-section of the bonding interface: (a) 316 L on 1045 steel; (b) 316 L on 1045 steel with substrate preheating; (c) 316 L on P20 steel; (d) 316 L on P20 steel with substrate preheating; (e) magnification of heat affected zone (HAZ) microstructure of P20; (f) HAZ microstructure of P20 under preheating.

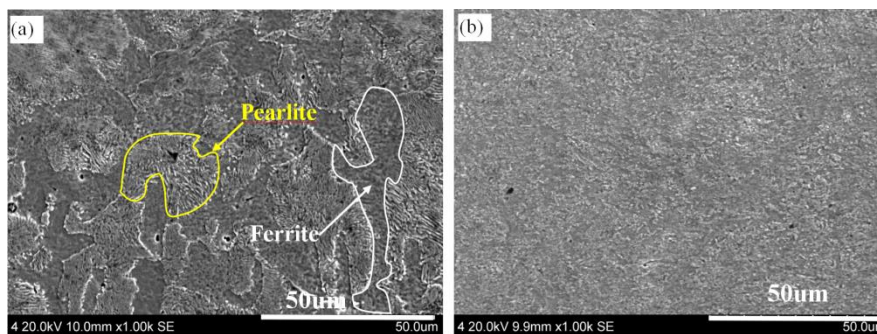


Figure 7. Unaffected microstructure of wrought substrate: (a) 1045 steel; (b) P20 steel.

The unaffected substrate microstructure of P20 steel is composed of tempered martensite, as shown in Figure 7b. The resultant microstructure at the HAZ experienced different degrees of tempering during laser deposition, which was also verified by Chen et al. [12]. Carbide precipitated and grew between martensitic lathes, and the carbide is marked by a purple circle in the highly magnified image

shown in Figure 6d. The HAZ microstructure had more carbide phases under substrate preheating, as shown in Figure 6c,d.

The compositional profiles of the interface between 316 L with 1045 and P20 steel are presented in Figure 8a,b, respectively. The compositional profiles of the interface under substrate preheating are shown in Figure 8c,d for comparison. The EDS testing lines are marked in Figure 6a–d. Because of composition difference between the lower alloyed substrate and the 316 L deposition layer, the contents of Cr, Ni and Fe elements tend to be found towards sharp decreases at the interface. The width of the composition variation zone is nearly equal to the width of the flat crystals near the fusion line. An EDS mapping performed at the fusion zone are shown in Figure 9, which demonstrates that the clear composition variation happened in the fusion line. The EDS mapping image was from specimens of laser deposition 316 L on 1045 steel without preheating (the testing region has been marked in Figure 6a), and the results of the other three specimens were similar in comparison (not shown to avoid repetition). The composition of the first deposition layer is homogeneous, no macrosegregation is found. This can be largely attributed to the sufficient mixing in the molten pool and the compositional difference between the substrate material and the deposition material. Macroseggregation might happen at the first deposition layer as mentioned by Liu [30]. The composition variation of different wrought materials under substrate preheating are the same as that without preheating, as shown in Figure 8c,d.

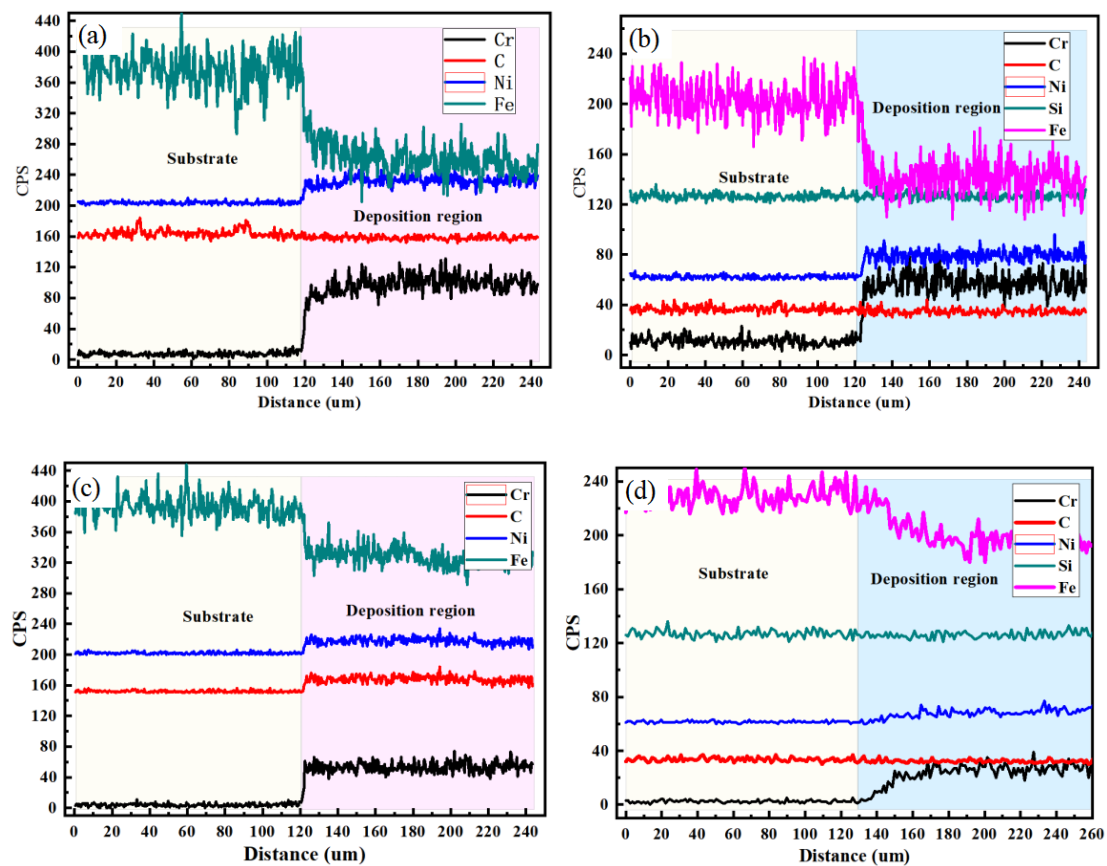


Figure 8. Line scanning analysis from substrate to deposition material without substrate preheating: (a) 1045 to 316 L; (b) P20 to 316 L; (c) 1045 to 316 L under preheating; (d) P20 to 316 L under preheating.

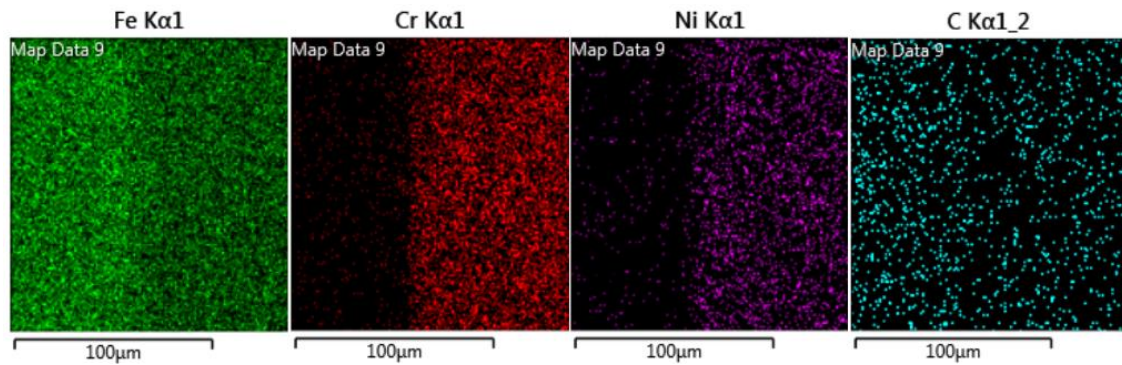


Figure 9. EDS map distribution of elements.

3.4. Tensile Properties

Figure 10 shows the stress–strain curves of specimens selected from LMD built from 316 L with wrought 1045 and P20 steel. The hybrid samples of 316 L/1045 steel cracked under a lower stress level. At the same time, there are large differences in mechanical properties among samples 1, 2, 3. Under substrate preheating, the average ultimate strength of hybrid forming specimens increases from 390 MPa to 557 MPa, and the average elongation increases from 3.8% to 37.3% as shown in Figure 11a. The weakness of tensile properties is correlated with the interface cracks. However, the stress–strain curve of 316 L/P20 steel hybrid specimens is similar, whether or not the substrate preheating was done, as shown in Figure 10b. The average ultimate tensile strength and elongation of hybrid specimens of 316 L with P20 steel are 565.3 MPa and 35.9% respectively, while this changes to 550 MPa and 32% under substrate preheating, as shown in Figure 11b.

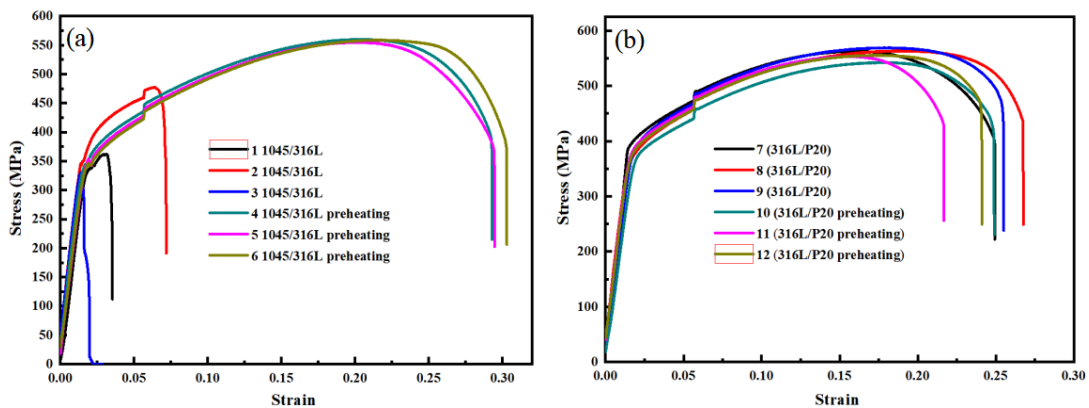


Figure 10. Stress–strain curve of laser metal deposition (LMD) built 316 L with wrought: (a) 1045 steel; (b) P20 steel.

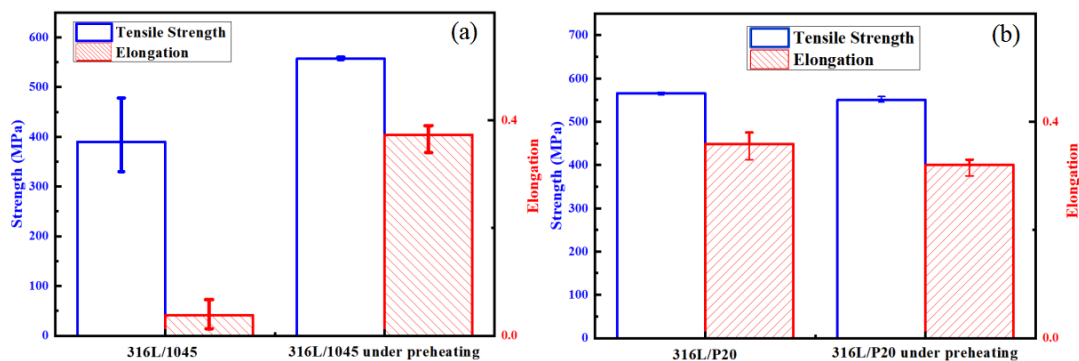


Figure 11. Static mechanical properties of different hybrid-processed samples: (a) 1045 with 316 L; (b) P20 with 316 L.

Figure 12 shows the hybrid formed plate tensile samples. The fracture surfaces of the tensile test specimens are presented in Figure 13. The white line in Figure 12 represents the interface of 316 L and substrate, and the shrinkage of the neck is presented in a large magnified image. Fractures of 316 L with 1045 steel are located in the interface without substrate preheating, whereas the location of the fracture changes to the LMD zone under substrate preheating. All fractures of 316 L with P20 steel specimens are in the LMD zone, despite the fractures near the interface. Neck contraction is found on samples which did not crack in the interface, as shown in Figure 12b–d.

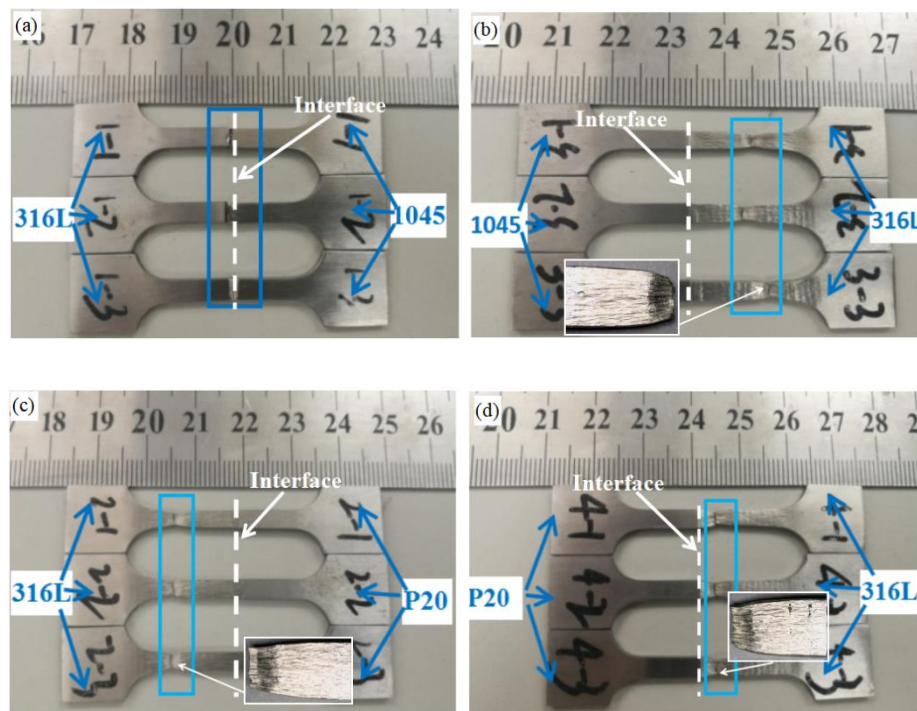


Figure 12. Hybrid formed plate tensile samples: (a) 316 L with 1045 steel; (b) 316 L with 1045 steel under preheating; (c) 316 L with P20 steel; (d) 316 L with P20 steel under preheating.

The resulting mechanical properties verify that the tensile strength of hybrid formed specimens with different substrates are very different. During the laser metal deposition process, some defects might form as a result of insufficient bonding, which deteriorates the adhesion properties. In this study, the 316 L and 1045 steel hybrid samples keep the interface bond characteristics safe under substrate preheating, which increases the bonding properties more so than without preheating. Under substrate preheating the deposition layer is smooth and wide, which will promote adhesion properties under the scanning method in the same hatch space. However, the mechanical properties of the hybrid specimens of 316 L with P20 steel were similar between different substrate temperatures, because no defects appeared on the interface zone without substrate preheating. The deposition width on 1045 steel was slightly smaller than P20 steel on the same parameter, as verified in Figure 2. As a result, the hybrid samples of 316 L and P20 can realize safe interface bonding even without the help of substrate preheating.

The tensile strength properties of hybrid forming 316 L with conventional manufacturing steel and without interface defects are found to be comparable to that of the laser metal deposition 316 L in the literature [29], which has ultimate tensile strength (540–625 MPa) and elongation (35–85%). The tensile strength of wrought 1045 steel and P20 steel is above 600 MPa and 1250 MPa, respectively. Additionally, the fracture of hybrid specimens occurs on the weakest position on the 316 L side, away from the interface.

Representative fractographs of the tensile specimens are shown in Figure 13. Flat fracture surface is shown in Figure 13a, which was caused by a crack formed during the laser metal deposition. The brittle fracture with dimple gliding fracture is shown in Figure 13b. Some micro cracks are discovered on the fracture surface. Conversely, the fracture surface under substrate preheating shows a dimpled ductile mode of tensile failure. The voids of unmelted powders in the laser metal deposition specimens could be avoided by using more laser power, however excessive heat input would also result in severe deformation of the wrought substrate. The fracture surfaces of 316 L with P20 steel, conversely, are ductile fracture mode free from the influence of substrate preheating. The dimple size observed on the fracture surface is similar. Some voids were also found, which were caused by incomplete melted powder, as mentioned by Sun et al. [14] and Yadollahi et al. [31]. The fracture surfaces are consistent with tensile properties as shown in Figures 10 and 11.

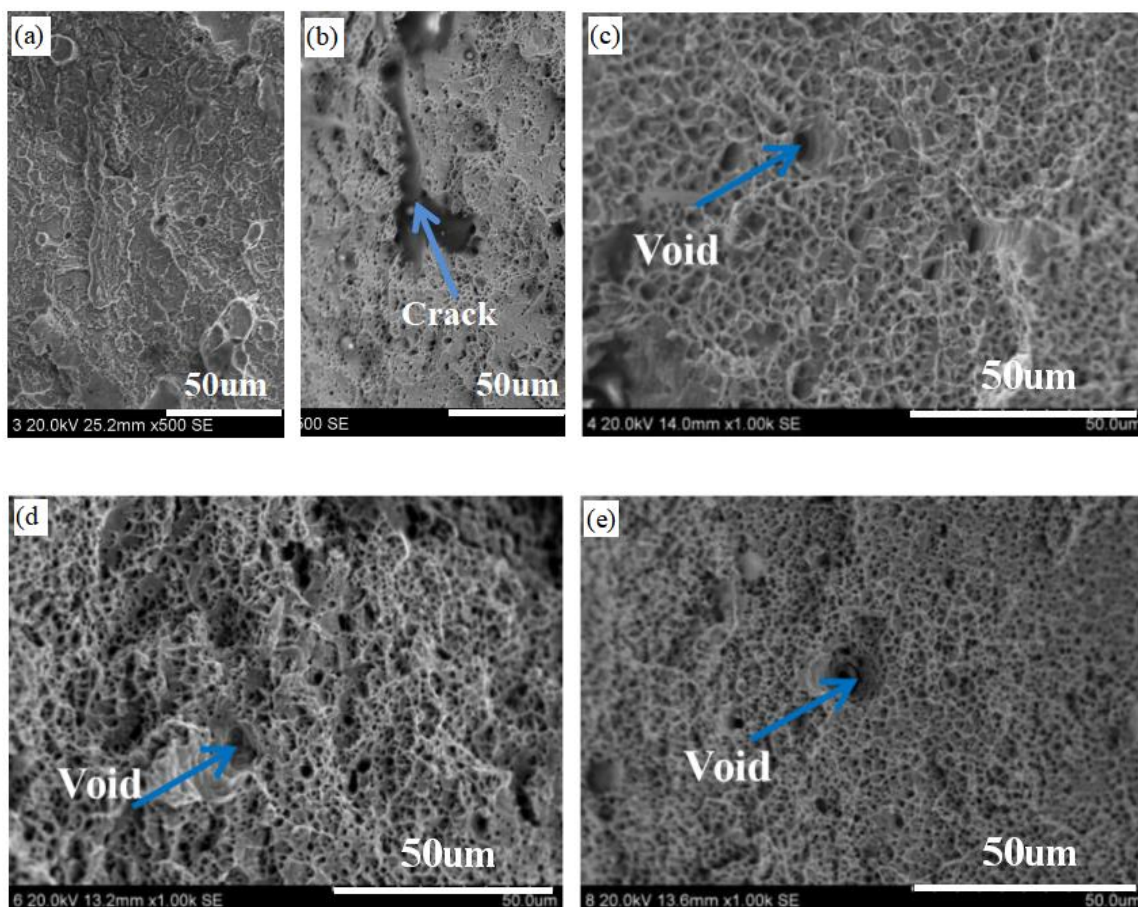


Figure 13. Scanning electron microscopy photos of the fracture surface of the specimen: (a) flat fracture surface of 316 L with 1045; (b) brittle fracture with dimple gliding fracture of 316 L with 1045; (c) 316 L with 1045 under preheating; (d) 316 L with P20, (e) 316 L with P20 under preheating.

3.5. Microhardness Distribution

The microhardness distributions along the building direction of the laser metal deposition 316 L on P20 and 1045 steel are given in Figure 14a,b, respectively. A schematic about the test point of hardness distribution is also shown. The mean hardness values of 316 L deposition zones for all specimens are around 200 HV_{0.2}. In addition, hardness distribution of different deposition layers is similar. However, sharp changes in hardness are found in the interface between different materials. The substrate HAZ hardness shows a different transformation phenomenon. The hardness of 1045 steel increases, while the HAZ hardness of P20 steel decreases, when comparing the affected substrate.

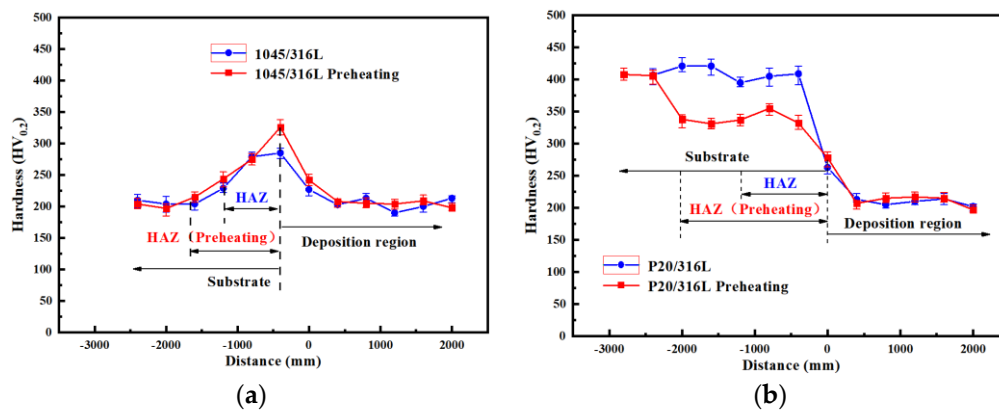


Figure 14. Microhardness profiles along depth direction on the transverse cross section: (a) from 1045 substrate to 316 L steel; (b) from P20 substrate to 316 L steel.

The influence of preheating on the substrate hardness is different between 1045 and P20 steel, which is closely related to the microstructure transformation. The hardness in 1045 steel HAZ region is increased, which is because the microstructure was refined and the proeutectoid ferrite disappeared during austenitization. The variation in characterization of substrate hardness is similar with different substrate temperatures. Conversely, the HAZ microstructure of P20 substrate experienced severe tempering after substrate preheating, which makes the HAZ hardness (300–330 HV_{0.2}) lower than without preheating. The decreasing width of the hardness region is correlated with the HAZ width without preheating. The hardness of P20 substrate without preheating is slightly decreased compared to the unaffected substrate hardness (higher than 400 HV_{0.2}).

The stress between first deposition layer and substance was usually the largest one among all the layers, and the residual stress at the border position of hybrid formed specimens was measured. The average value of residual stress in 316 L/1045 steel was 280 MPa, while after substrate preheating the stress decreased to 262 MPa. The average value of stress in 316 L/P20 steel specimens decreased from 303 MPa to 273 MPa under substrate preheating. Under substrate preheating, the stress of deposition and substrate was reduced, while in this research, the influence of preheating on the residual stress was small. The influence of substrate preheating on the thermal and residual stress will be discussed further by high-scale laser cladding in hybrid forming process. The preheating temperature higher than 200 °C might be more suitable to guarantee safe bonding and a lower stress level, but it is hard to achieve this in a large scale part.

4. Conclusions

The followings are significant conclusions which can be drawn from this study:

1. Under substrate preheating, the deposition width (W1) was increased and deposition height (H2) showed little difference. At the same time, the variation amplitude of deposition height (H2) as heat input increased was weakened, but the variation amplitude of deposition width W1 was broadened. In addition, the H2/W1 ratio was decreased, making the deposition layer surface smoother. Similar morphology variation was found with both 1045 and P20 substrates.
2. LMD 316 L formed metallurgically sound and dense bonding with 1045 steel substrate under substrate preheating, while defects were formed near the bonding interface without substrate preheating. LMD 316 L with P20 steel specimens have metallurgically bonding characteristic without defects under different substrate temperature. The microstructure of deposition layers was similar between different substrate materials and temperatures.
3. The adhesion properties of hybrid formed 316 L with 1045 were obviously decreased without substrate preheating, and brittle fractures of 316 L with 1045 steel were located in the interface without substrate preheating. The adhesion properties of hybrid formed 316 L with P20 had

no relationship with substrate preheating because of the metallurgic bonding characteristic in the interface. The difference between P20 and 1045 steel substrate was mainly because of geometrical characterization of deposition layers under the same processing parameters. The level of hybrid samples without interface defects can reach laser deposition 316 L tensile properties. When combining laser metal deposition with conventional metal forming for an easy-forming alloy, preheating realized safe interface bonding, but was not necessary.

4. The sharp changes in hardness were found in the interface between different materials. The substrate HAZ hardness showed different transformation phenomenon.

Author Contributions: Conceptualization and methodology, Y.Z. and Z.W.; software, Z.H. and H.Z.; formal analysis, Y.Z.; investigation, Z.W.; resources, J.Z.; data curation, Z.W., Z.H. and H.Z.; writing—original draft preparation, Y.Z.; writing—review and editing, Z.W.; supervision, J.Z.; project administration, J.Z.; funding acquisition, Y.Z. All authors have read and agreed to the published version of the manuscript.

Funding: This research was funded by the National Natural Science Foundation of China, grant number 51805526 and the National Key Research and Development Program of China (2018YFB1105802).

Acknowledgments: The authors want to acknowledge Shenyang Institute of Automation Chinese Academy of Sciences for technical support.

Conflicts of Interest: The authors declare no conflict of interest.

References

1. Merklein, M.; Junker, D.; Schaub, A.; Neubauer, F. Hybrid additive manufacturing technologies—An analysis regarding potentials and applications. *Phys. Procedia* **2016**, *83*, 549–559. [\[CrossRef\]](#)
2. Cortina, M.; Arrizubieta, J.I.; Calleja, A.; Ukar, E.; Alberdi, A. Case study to illustrate the potential of conformal cooling channels for hot stamping dies manufactured using hybrid process of Laser Metal Deposition (LMD) and milling. *Metals* **2018**, *8*, 102. [\[CrossRef\]](#)
3. Hölker-Jäger, R.; Tekkaya, A.E. Additive manufacture of tools and dies for metal forming. *Laser Addit. Manuf.* **2017**, 439–464. [\[CrossRef\]](#)
4. Nowotny, S.; Spatzier, J.; Kubisch, F.; Scharek, S.; Ortner, J.; Beyer, E. Repair of erosion defects in gun barrels by direct laser deposition. *J. Therm. Spray Technol.* **2012**, *21*, 1173–1183. [\[CrossRef\]](#)
5. Song, L.; Zeng, G.; Xiao, H.; Xiao, X.; Li, S. Repair of 304 stainless steel by laser cladding with 316L stainless steel powders followed by laser surface alloying with WC powders. *J. Manuf. Process.* **2016**, *24*, 116–124. [\[CrossRef\]](#)
6. Cui, W.; Li, W.; Chen, W.T.; Liou, F. Laser Metal Deposition of an AlCoCrFeNiTi0.5 High-Entropy Alloy Coating on a Ti6Al4V Substrate: Microstructure and Oxidation Behavior. *Crystals* **2020**, *10*, 638. [\[CrossRef\]](#)
7. Zhu, Y.; Li, J.; Tian, X.; Wang, H.; Liu, D. Microstructure and mechanical properties of hybrid fabricated Ti-6.5 Al-3.5 Mo-1.5 Zr-0.3 Si titanium alloy by laser additive manufacturing. *Mater. Sci. Eng. A* **2014**, *607*, 427–434. [\[CrossRef\]](#)
8. Kim, D.K.; Woo, W.; Kim, E.Y.; Choi, S.H. Microstructure and mechanical characteristics of multi-layered materials composed of 316L stainless steel and ferritic steel produced by direct energy deposition. *J. Alloy. Compd.* **2019**, *774*, 896–907. [\[CrossRef\]](#)
9. Kim, H.; Liu, Z.; Cong, W.; Zhang, H.C. Tensile Fracture Behavior and Failure Mechanism of Additively-Manufactured AISI 4140 Low Alloy Steel by Laser Engineered Net Shaping. *Materials* **2017**, *10*, 1283. [\[CrossRef\]](#)
10. Lai, Q.; Abrahams, R.; Yan, W.; Qiu, C.; Mutton, P.; Paradowska, A.; Soodi, M. Investigation of a novel functionally graded material for the repair of premium hypereutectoid rails using laser cladding technology. *Compos. Part B Eng.* **2017**, *130*, 174–191. [\[CrossRef\]](#)
11. Wang, Q.; Zhang, S.; Zhang, C.H.; Wu, C.; Wang, J.; Chen, J.; Sun, Z. Microstructure evolution and EBSD analysis of a graded steel fabricated by laser additive manufacturing. *Vacuum* **2017**, *141*, 68–81. [\[CrossRef\]](#)
12. Chen, J.Y.; Conlon, K.; Xue, L.; Rogge, R. Experimental study of residual stresses in laser clad AISI P20 tool steel on pre-hardened wrought P20 substrate. *Mater. Sci. Eng. A* **2010**, *527*, 7265–7273. [\[CrossRef\]](#)
13. Liu, J.; Li, J.; Cheng, X.; Wang, H. Effect of dilution and macrosegregation on corrosion resistance of laser clad AerMet100 steel coating on 300M steel substrate. *Surf. Coat. Technol.* **2017**, *325*, 352–359. [\[CrossRef\]](#)

14. Sun, G.; Zhou, R.; Lu, J.; Mazumder, J. Evaluation of defect density, microstructure, residual stress, elastic modulus, hardness and strength of laser-deposited AISI 4340 steel. *Acta Mater.* **2015**, *84*, 172–189. [[CrossRef](#)]
15. Bambach, M.D.; Bambach, M.; Sviridov, A.; Weiss, S. New process chains involving additive manufacturing and metal forming—a chance for saving energy? *Procedia Eng.* **2017**, *207*, 1176–1181. [[CrossRef](#)]
16. Juhasz, M.; Tiedemann, R.; Dumstorff, G.; Walker, J.; Du Plessis, A.; Conner, B.; MacDonald, E. Hybrid directed energy deposition for fabricating metal structures with embedded sensors. *Addit. Manuf.* **2020**, *35*, 101397. [[CrossRef](#)]
17. Hassen, A.A.; Noakes, M.; Nandwana, P.; Kim, S.; Kunc, V.; Vaidya, U.; Nycz, A. Scaling Up metal additive manufacturing process to fabricate molds for composite manufacturing. *Addit. Manuf.* **2020**, *32*, 101093. [[CrossRef](#)]
18. He, Y.; Wei, J.; Liu, J.; Wang, X.; Wang, Y.; He, L. Experimental study on the fabrication profile and mechanical properties by substrate-inclined angle using laser melting deposition (LMD) integrating with the substrate of stainless steel. *Opt. Laser Technol.* **2020**, *125*, 106038. [[CrossRef](#)]
19. Shim, D.S.; Baek, G.Y.; Lee, E.M. Effect of substrate preheating by induction heater on direct energy deposition of aisi m4 powder. *Mater. Sci. Eng. A* **2017**, *682*, 550–562. [[CrossRef](#)]
20. Li, X.P.; Roberts, M.; Liu, Y.J.; Kang, C.W.; Huang, H.; Sercombe, T.B. Effect of substrate temperature on the interface bond between support and substrate during selective laser melting of Al–Ni–Y–Co–La metallic glass. *Mater. Des. (1980–2015)* **2015**, *65*, 1–6. [[CrossRef](#)]
21. Lai, Q.; Abrahams, R.; Yan, W.; Qiu, C.; Mutton, P.; Paradowska, A.; Fang, X.; Soodi, M.; Wu, X. Effects of preheating and carbon dilution on material characteristics of laser-cladded hypereutectoid rail steels. *Mater. Sci. Eng. A* **2018**, *712*, 548–563. [[CrossRef](#)]
22. Wang, Z.; Zhao, J.; Zhao, Y.; Zhang, H. Microstructure and Microhardness of Laser Metal Deposition Shaping K465/Stellite-6 Laminated Material. *Metals* **2017**, *7*, 512. [[CrossRef](#)]
23. Farahmand, P.; Kovacevic, R. An experimental–numerical investigation of heat distribution and stress field in single-and multi-track laser cladding by a high-power direct diode laser. *Opt. Laser Technol.* **2014**, *63*, 154–168. [[CrossRef](#)]
24. Huang, Y.; Khamesee, M.B.; Toyserkani, E.A. Comprehensive analytical model for laser powder-fed additive manufacturing. *Addit. Manuf.* **2016**, *12*, 90–99. [[CrossRef](#)]
25. Liu, H.; Hao, J.; Han, Z.; Yu, G.; He, X.; Yang, H. Microstructural evolution and bonding characteristic in multi-layer laser cladding of NiCoCr alloy on compacted graphite cast iron. *J. Mater. Process. Technol.* **2016**, *232*, 153–164. [[CrossRef](#)]
26. Pham, M.S.; Dovggy, B.; Hooper, P.A. Twinning induced plasticity in austenitic stainless steel 316L made by additive manufacturing. *Mater. Sci. Eng. A* **2017**, *704*, 102–111. [[CrossRef](#)]
27. Chen, X.; Li, J.; Cheng, X.; He, B.; Wang, H.; Huang, Z. Microstructure and mechanical properties of the austenitic stainless steel 316L fabricated by gas metal arc additive manufacturing. *Mater. Sci. Eng. A* **2017**, *703*, 567–577. [[CrossRef](#)]
28. Rashid, R.R.; Abaspour, S.; Palanisamy, S.; Matthews, N.; Dargusch, M.S. Metallurgical and geometrical characterisation of the 316L stainless steel clad deposited on a mild steel substrate. *Surf. Coat. Technol.* **2017**, *327*, 174–184. [[CrossRef](#)]
29. Farshidianfar, M.H.; Khajepouh, A.; Gerlich, A. Real-time monitoring and prediction of martensite formation and hardening depth during laser heat treatment. *Surf. Coat. Technol.* **2017**, *315*, 326–334. [[CrossRef](#)]
30. Liu, J.; Li, J.; Cheng, X.; Wang, H. Microstructures and tensile properties of laser cladded AerMet100 steel coating on 300 M steel. *J. Mater. Sci. Technol.* **2018**, *34*, 643–652. [[CrossRef](#)]
31. Yadollahi, A.; Shamsaei, N.; Thompson, S.M.; Denver, W.S. Effects of process time interval and heat treatment on the mechanical and microstructural properties of direct laser deposited 316L stainless steel. *Mater. Sci. Eng. A* **2015**, *644*, 171–183. [[CrossRef](#)]

